

Cite this: DOI:00.0000/xxxxxxxxxx

Prediction of induced magnetism in 2D Ti₂C based MXene by manipulating the mixed surface functionalization and metal substitution computed by xTB model Hamiltonian of the DFTB method †

Taoufik Sakhraoui,*^a Frantisek Karlicky,^aReceived Date
Accepted Date

DOI:00.0000/xxxxxxxxxx

We employed the recently developed density functional tight binding (DFTB) method's Hamiltonian, GFN1-xTB, for modeling the mixed termination in Ti₂C MXene, namely three types of termination by combining -O and -OH, -O and -F, as well as -F and -OH. We demonstrated that the approach yields reliable predictions for electronic and magnetic properties of such MXenes. The first highlighted result is that the mixed surface functionalization in Ti₂CA_xB_y MXene induces spin polarization with diverse magnetic alignments, including ferromagnetism and two types of antiferromagnetism. We further identified the magnetic alignment for the investigated MXene in terms of the compositions of the terminal groups. Moreover, the effect of the transition metal (Ti) substituted by the Sc atom on the electronic and magnetic properties were also investigated. We found that the studied systems maintain the magnetism and the metallic characteristics. A magnetic transition from antiferromagnetic (AFM) to ferrimagnetic (FiM) ordering was found for ScTi₁₅C₈F₈(OH)₈ and ScTi₁₅C₈F₁₂(OH)₄ compounds. Finally, we proved that incorporating the Sc atom into the lattice of Ti₂CO₂ and mixed surface termination Ti₂CA_xB_y is an effective strategy to induce magnetism. Our study may provide a new potential application for designing MXene-based spintronics.

1 Introduction

In recent years, MXenes M_nX_{n-1}T_x (1 ≤ n ≤ 4 and x ≤ 2), a family of transition-metal carbide and nitride materials, consist of transition metals (M) including Sc, Ti, V, Cr, Mn, Y, Zr, Nb, Mo, Hf, Ta, carbon or nitrogen (X), and the surface termination (T), devoted great attention¹⁻⁴. MXenes^{2,5}, as two-dimensional (2D) materials, have been experimentally synthesized⁶ by using various experimental techniques, such as simple oxidation⁷, nuclear magnetic resonance (NMR) spectroscopy^{4,8}, neutron diffraction⁹, and STEM-EELS¹⁰ and theoretically predicted¹¹⁻¹⁶. They have attracted great interest due to their excellent mechanical, electrical, optical, and electrochemical properties¹⁷⁻¹⁹, which have potential applications in various fields²⁰⁻²³ such as sensors, catalysis, energy storage, and nanoelectronics. Among MXenes, Ti₂C is one of the most widely investigated, it was prepared by etching the Ti₂AlC MAX phase²⁴. The arrangement between Ti and C atoms in Ti₂C forms the honeycomb structure where carbon is sandwiched by two titanium. Moreover, during the etching process,

Ti₂C may be functionalized by F, O or OH forming Ti₂CT₂ (T = F, O, OH)^{3,4,11,25,26}. In these structures, the C atoms are still sandwiched between the Ti atoms, and the T atoms on both terminals occupy the top site of bottom titanium on both sides^{3,11,25}. We note that previous literature reveals that surface terminal groups such as -Cl, -Br, -I, -S, -Te, -NH, -H, -BrI, and -ClBrI²⁷⁻³¹ were identified in several MXenes too. It was recently predicted that the bare Ti₂C MXene prefers a magnetic ground state that corresponds to antiferromagnetic (AFM) coupled to ferromagnetic (FM) layers³². Whereas, the magnetic ground state of Ti₂C can be switched from AFM to nonmagnetic (NM) state by full surface termination by O, F and OH³³⁻³⁵. On the other hand, the control of the surface functionalization by O, OH, and F in MXenes may allow the control of the material properties. From experimental point of view, it has been shown that Ti₃C₂ showed a mixture of terminations by F, O, and OH^{4,26,36} and that the composition depends on etching process, i.e., O functionalization dominates when using LiF and HCl^{4,36} and F functionalization dominates when using HF⁴. MXenes naturally lose their inversion symmetry upon mixed surface functionalization, thereby opening up new design opportunities for controlling their physical properties. However, a proper understanding of the effect of the mixed functionalization of the Ti₂C surface on the electronic and mag-

^a Department of Physics, Faculty of Science, University of Ostrava, 701 03 Ostrava, Czech Republic

* E-mail: taoufik.sakhraoui@osu.cz

† Electronic Supplementary Information (ESI) available: [details of any supplementary information available should be included here]. See DOI:

netic properties is still missing. Furthermore, to the extent of our knowledge, computational^{26,37,38} and experimental^{4,36} studies did not treat magnetism in mixed terminated Ti_2C . M. Bagheri *et al.* reported results for the Fermi surfaces of titanium carbide and nitride MXenes (Ti_3C_2 , Ti_2C , Ti_4N_3 , and Ti_2N) as a function of the mixed O and OH terminal groups³⁷. T. Schultz *et al.* reported a comparative study of a combination of ultraviolet photoemission spectroscopy (UPS), X-ray photoelectron spectroscopy (XPS), and inverse photoemission spectroscopy (IPES) measurements of $\text{Ti}_3\text{C}_2\text{T}_x$ with density functional theory (DFT) calculations³⁹.

The use of DFT for materials properties prediction is mostly applicable to small systems because of the high computational cost. This is a significant limitation because advances in MXenes require the study of larger systems, such as the influence of the concentration of vacancies and defects in the compound on the electronic and magnetic properties. Semiempirical methods, such as density functional tight binding (DFTB), may give a perfect and complementary platform⁴⁰. DFTB has been used to investigate numerous systems including solid state⁴¹, molecular and biological systems⁴², titanium-based materials,^{14,43} and 2D materials^{14,44,45}. The applicability of DFTB method requires the availability of parameter sets for all pairs of atoms present in the system^{46,47}. This approach has been already tested on the 2D materials⁴⁸ and it was applied for defected Ti_2CO_2 MXene¹⁴. However, when compared with the exact eigenstates and eigenvalues from the exact calculations in finite Hubbard model⁴⁹, the tight binding case is a rather crude approximation. One can use exact calculations of local many body effects by incorporating the Hubbard or Heisenberg models in various structural geometries, as in refs.^{50–52}. The Geometries, Frequencies, and Non-covalent interactions Tight Binding (GFN1-xTB) Hamiltonian presents a good alternative for electronic structure and magnetic properties calculations. GFN1-xTB Hamiltonian⁵³ provides parameters for elements up to $Z \leq 86$, and it was recently supported by DFTB+ code⁵⁴. Moreover, the consistency between xTB and DFT functionals is already shown in recent publications^{55,56}. The reader may refer to the following refs.^{53,57,58} for more details about xTB and comparison to other methods.

In the present work, we employed GFN1-xTB version of the xTB Hamiltonian to investigate the electronic and magnetic properties of $\text{Ti}_2\text{CA}_x\text{B}_y$ ($A, B = \text{O}, \text{F}$ and OH and x and $y = 0.5, 1.0$ and 1.5 ; $x + y = 2$) and to study the effect of metal substitution in mixed surface termination Ti_2C -based MXene.

2 Methods

The xTB calculations presented in this study were performed using DFTB+ package^{54,59} with the implementation of the GFN1-xTB method⁵³. The GFN1-xTB Hamiltonian is well described in refs^{53,57} and⁵⁵. xTB combines high accuracy from DFT-based parameters with the reduced computational cost of standard tight-binding methods. This technique is thus advantageous for describing large supercells. It has near DFT precision in electronic structure calculations while being significantly faster than DFT^{53,55,57,58,60}. A conjugate gradient algorithm was used for geometry optimization imposing a maximum force of 10^{-4} au. The self-consistent calculations were considered to be converged

when the difference in the total energy did not exceed 10^{-3} au. To obtain converged electron energy values, a Fermi distribution was used for the system at an electron temperature of 700 K. The total energy is calculated by integrating over the Brillouin zone with a Gamma-centered k-mesh of $6 \times 9 \times 1$ Monkhorst-Pack⁶¹ grid for the mixed terminal groups in the $2 \times 1 \times 1$ - Ti_2C supercell (i.e., $\text{Ti}_4\text{C}_2\text{A}_a\text{B}_b$, where A and B are the F, O, and OH terminal groups and $a + b = 4$). The Ti substitution by Sc in $\text{Ti}_2\text{CA}_x\text{B}_y$ is modeled by a $2 \times 2 \times 1$ supercell and $1 \times 6 \times 1$ grid. Finally, to study the effect of the Ti substitution by Sc in Ti_2CO_2 , we used a $5 \times 5 \times 1$ supercell ($\text{Ti}_{50}\text{C}_{25}\text{O}_{50}$) and a Γ -point only setup. In order to prevent interaction with its own images, the out-of-plane bounding box was set to 20 Å. Some additional DFT calculations were performed using Quantum Espresso (QE) package, see ESI for more details.

3 Results and discussions

To address the full range of mixed (O/OH, O/F and F/OH) surface termination compositions in the $\text{Ti}_2\text{CA}_x\text{B}_y$ ($A, B = \text{O}, \text{F}, \text{OH}$ and $x, y = 0.5, 1.0, 1.5$; $x + y = 2$), we used a $2 \times 1 \times 1$ - Ti_2C supercell (i.e., $\text{Ti}_4\text{C}_2\text{A}_a\text{B}_b$, where $a + b = 4$). In $\text{Ti}_2\text{CA}_{1.5}\text{B}_{0.5}$, $\text{Ti}_2\text{CA}_{1.0}\text{B}_{1.0}$ and $\text{Ti}_2\text{CA}_{0.5}\text{B}_{1.5}$ compositions, there are 3, 2 and 1 sites occupied by A termination and 1, 2 and 3 sites occupied by B termination, respectively. Surface composition is shown in Fig. 1.

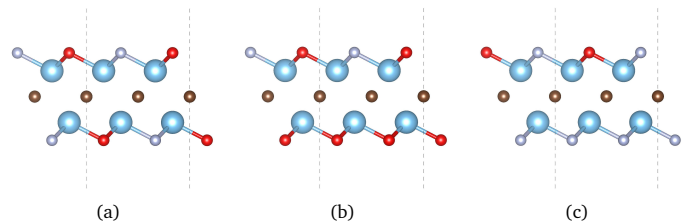


Fig. 1 Mixed functionalization in $\text{Ti}_2\text{CA}_x\text{B}_y$ ($A, B = \text{O}, \text{F}, \text{OH}$). (a) $\text{Ti}_2\text{CA}_{1.0}\text{B}_{1.0}$, (b) $\text{Ti}_2\text{CA}_{1.5}\text{B}_{0.5}$, and (c) $\text{Ti}_2\text{CA}_{0.5}\text{B}_{1.5}$. Blue, red, light gray and chocolate balls represent Ti, A, B and C atoms, respectively.

3.1 Electronic structure and magnetic properties of mixed $\text{Ti}_2\text{CA}_x\text{B}_y$ MXene

In addition to the FM arrangement, three different AFM arrangements are considered here, including an interlayer antiferromagnetism (AFM2), and two possible intralayer antiferromagnetic arrangements (AFM1 and AFM3) as shown in Fig. 2. For AFM1, the Ti atoms on one side are in the same spin orientation with the diagonal Ti atoms on the other side, while in AFM2, the spin orientations of metal atoms on one side are opposite to those on the other side. In AFM3, the Ti atoms on one side are in the same spin orientation as the corresponding Ti atoms on the other side. Here, the calculations are based on the ground state of various configurations.

Table 1 Calculated magnetic energy difference ($E_{\text{FM},\text{AFM}_j(j=1,2,3)} - E_{\text{FM}}$) and magnetic moments in of mixed $\text{Ti}_2\text{CA}_x\text{B}_y$ ($A, B = \text{O, F, OH}$). The ground state energy is marked in bold. For comparison to DFT, the PBE results using Quantum Espresso code are listed in the table S1. The magnetic configurations here are starting guesses, then the system is relaxing to its self-consistent magnetic solution.

Initial magnetic state	Magnetic energy difference (meV)				Total magnetic moment (μ_B/cell)			
	FM	AFM1	AFM2	AFM3	FM	AFM1	AFM2	AFM3
$\text{Ti}_2\text{CO}_1(\text{OH})_1$	0.00	0.00	36.30	36.30	2.00	2.00	0.00 (AFM2)	0.00 (AFM2)
$\text{Ti}_2\text{CO}_{1.5}(\text{OH})_{0.5}$	0.00	0.00	89.40	0.00	1.00	1.00	0.40	1.00
$\text{Ti}_2\text{CO}_{0.5}(\text{OH})_{1.5}$	0.00	23.80	24.10	6.30	2.31	3.00	0.28	1.24
$\text{Ti}_2\text{CO}_1\text{F}_1$	0.00	0.00	61.10	60.20	2.00	2.00	0.00 (AFM2)	0.00 (AFM3)
$\text{Ti}_2\text{CO}_{1.5}\text{F}_{0.5}$	0.00	0.00	0.00	0.00	1.00	1.00	1.00	1.00
$\text{Ti}_2\text{CO}_{0.5}\text{F}_{1.5}$	0.00	128.10	194.10	176.70	3.00	0.96	0.06	2.21
$\text{Ti}_2\text{CF}_1(\text{OH})_1$	0.00	200.20	-29.60	159.00	4.00	0.48	0.00 (AFM2)	0.00 (AFM3)
$\text{Ti}_2\text{CF}_{1.5}(\text{OH})_{0.5}$	0.00	44.20	-165.40	16.80	3.34	0.17	0.00 (AFM2)	0.06
$\text{Ti}_2\text{CF}_{0.5}(\text{OH})_{1.5}$	0.00	263.00	148.20	108.30	4.00	1.55	2.00	2.00

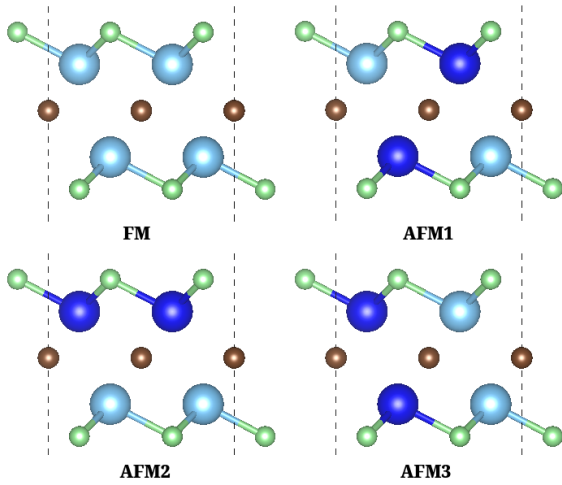


Fig. 2 Magnetic configurations of mixed $\text{Ti}_2\text{CA}_x\text{B}_y$ MXene. Green and chocolate colors represent the terminal group (O, F, OH) and C atoms, respectively. The dark and light blue balls denote Ti atoms with opposite spin orientation.

The electronic and magnetic properties of $\text{Ti}_2\text{CA}_x\text{B}_y$ ($A, B = \text{O, F, OH}$) were explored. To determine the ground magnetic states of the considered composition of the terminal groups, the total energies of the possible magnetic alignments, including FM and AFM states, and their corresponding total magnetic moments were calculated and listed in Table 1. We notice that the lowest energy has been found for FM state for most of the structures, except for $\text{Ti}_2\text{CF}_1(\text{OH})_1$ and $\text{Ti}_2\text{CF}_{1.5}(\text{OH})_{0.5}$, which prefer AFM2 alignment, where Ti atoms on one side are anti-ferromagnetically coupled with the Ti atoms on the other side. The energy differences between FM and AFM2 states in $\text{Ti}_2\text{CF}_1(\text{OH})_1$ and $\text{Ti}_2\text{CF}_{1.5}(\text{OH})_{0.5}$ are 29.6 and 165.4 meV/unit cell, respectively. We note that the energetic difference is in the order of a few meV, this result is confirmed by DFT calculations using Quantum Espresso code (DFT-PBE results are listed in Table S1).

To understand the effects of surface termination composition and ordering on the electronic and magnetic properties of the studied systems, we plot the density of states for $\text{Ti}_2\text{CA}_x\text{B}_y$ ($A, B = \text{O, F, OH}$) in Fig. 3. For all considered systems, regardless of the composition and ordering of O, F and OH terminations, $\text{Ti}_2\text{CA}_x\text{B}_y$ exhibit nearly half-metallic ferromagnetism. There are many energy states crossing the Fermi level for the spin-up chan-

nels, indicating their metallic character, nonetheless, the spin-down channels are semiconducting. However, for $\text{Ti}_2\text{CF}_1(\text{OH})_1$ and $\text{Ti}_2\text{CF}_{1.5}(\text{OH})_{0.5}$, as shown in Fig. 3, both systems are metallic and the spin polarization is shown in an antiferromagnetic ordering, and thus they are AFM metals. The anti-parallel spin alignment of the Ti atoms on one side and the Ti atoms on the other side results in the zero magnetic moment of the whole system and the AFM2 state in both $\text{Ti}_2\text{CF}_1(\text{OH})_1$ and $\text{Ti}_2\text{CF}_{1.5}(\text{OH})_{0.5}$. Our results reveal that the absolute value of the local magnetic moments of Ti atoms in FM- $\text{Ti}_2\text{CF}_{0.5}(\text{OH})_{1.5}$ are in the same range compared to those in AFM magnetic ground states of $\text{Ti}_2\text{CF}_1(\text{OH})_1$ and $\text{Ti}_2\text{CF}_{1.5}(\text{OH})_{0.5}$. Moreover, we found that the total magnetic moment values are sensitive to the terminal group composition. The total magnetic moments of the FM structures range from $1 \mu_B$ in $\text{Ti}_2\text{CO}_{1.5}(\text{OH})_{0.5}$ to $4 \mu_B$ in $\text{Ti}_2\text{CF}_{0.5}(\text{OH})_{1.5}$. In addition, $\text{Ti}_2\text{CF}_x(\text{OH})_y$ compositions possess the highest magnetic moments compared to $\text{Ti}_2\text{CO}_x\text{F}_y$ and $\text{Ti}_2\text{CO}_x(\text{OH})_y$. Therefore, the varying concentration of O, F and OH provides an effective way to control the spin-polarization. Moreover, the magnetic moments of $\text{Ti}_2\text{CA}_x\text{B}_y$ are mainly contributed by the Ti atoms and their values depend on the mixing ratio.

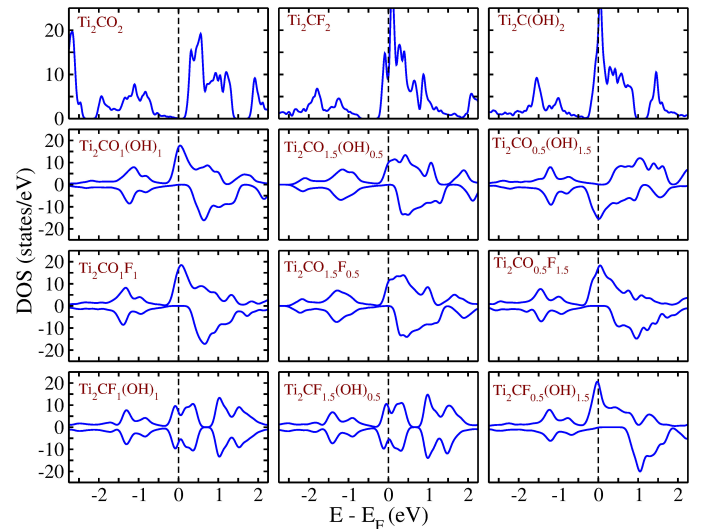


Fig. 3 Calculated total density of states (DOS) of bare Ti_2CA_2 and $\text{Ti}_2\text{CA}_x\text{B}_y$ ($A, B = \text{O, F, OH}$) MXenes with different mixed terminations in their ground-state configurations. The Fermi level is set to zero.

Based on the ground-state configurations of the studied materials, the partial magnetic moments are present in Fig. 4. We clearly see that $\text{Ti}_2\text{CO}_1(\text{OH})_1$ and $\text{Ti}_2\text{CO}_{1.5}(\text{OH})_{0.5}$ represent similar trends as $\text{Ti}_2\text{CO}_1\text{F}_1$ and $\text{Ti}_2\text{CO}_{1.5}\text{F}_{0.5}$, respectively, for all ranges of compositions. In $\text{Ti}_2\text{CO}_1(\text{OH})_1$ and $\text{Ti}_2\text{CO}_1\text{F}_1$, the magnetism is distributed over all Ti atoms with local magnetic moments of about 1, 0.5, 0.5, and 1 μ_B , respectively. For $\text{Ti}_2\text{CO}_{1.5}(\text{OH})_{0.5}$ and $\text{Ti}_2\text{CO}_{1.5}\text{F}_{0.5}$, a rapid increase of the spin moment going from Ti1 atom, where the local moment is almost zero, to Ti4 sites was seen. However, $\text{Ti}_2\text{CO}_{0.5}(\text{OH})_{1.5}$ and $\text{Ti}_2\text{CO}_{0.5}\text{F}_{1.5}$ show different behavior. In the case of $\text{Ti}_2\text{CF}_x(\text{OH})_y$, both $\text{Ti}_2\text{CF}_1(\text{OH})_1$ and $\text{Ti}_2\text{CF}_{1.5}(\text{OH})_{0.5}$ show an AFM2 ordering where the local magnetic moments are 1.6 μ_B for Ti1 and Ti2 atoms and -1.6 μ_B for Ti3 and Ti4 atoms. However, a FM alignment was observed for the $\text{Ti}_2\text{CF}_{0.5}(\text{OH})_{1.5}$ composition, where the local magnetic moments of Ti1 and Ti2 atoms have almost the same value of about 1.5 μ_B , while Ti3 and Ti4 atoms represent local magnetic moments of about 1.4 and 1.2 μ_B , respectively. Noteworthy that the local moments at the C1 and C2 atoms are almost zero for all compositions.

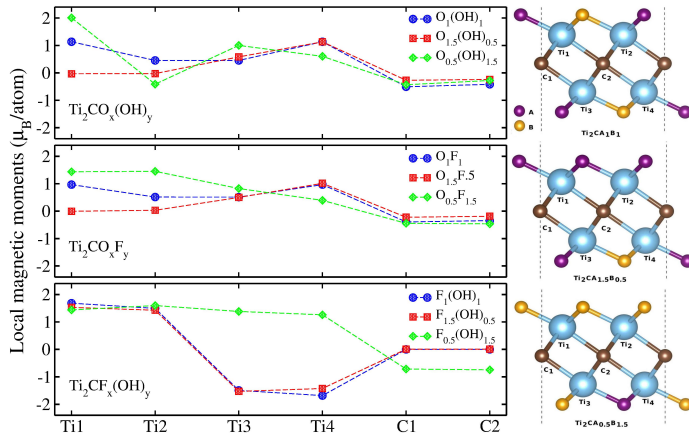


Fig. 4 Partial magnetic moment of different terminations in mixed $\text{Ti}_2\text{CA}_x\text{B}_y$ (A, B = O, F, OH) MXene in their ground-state configurations, $x, y=0.5, 1.0, 1.5$. Dashed lines are guide to the eye.

3.2 Substitution of one Ti by Sc in mixed surface termination MXene ($\text{Ti}_2\text{CA}_x\text{B}_y$)

To study the effect of the substitution of one Ti by Sc in mixed MXene, we used a $2 \times 2 \times 1$ - $\text{Ti}_2\text{CA}_x\text{B}_y$ supercell ($\text{ScTi}_{15}\text{C}_8\text{A}_a\text{B}_b$, $a+b=16$; i.e., 40 to 52 atoms depending on the terminal group composition). After relaxing the structures, the total magnetic moments of $2 \times 2 \times 1$ - $\text{Ti}_2\text{CA}_x\text{B}_y$ are calculated. The calculated total magnetic moments of $\text{ScTi}_{15}\text{C}_8\text{A}_a\text{B}_b$ ($a+b=16$) are listed in Table 2 and the corresponding local magnetic moments are listed in Table S2 and Table S3. We see that the total magnetic moments are relatively higher for the mixed F and OH terminal group compared to mixed O and F and mixed O and OH terminations, ranging from 5.00 μ_B/cell for $\text{ScTi}_{15}\text{C}_8\text{F}_{12}(\text{OH})_4$ to 15.06 μ_B/cell for $\text{ScTi}_{15}\text{C}_8\text{F}_4(\text{OH})_{12}$. The substitution of Sc atom in the mixed O and OH terminal group can induce lower magnetic moments of 7.04, 3.21 and 11.23 μ_B/cell for $\text{ScTi}_{15}\text{C}_8\text{O}_8(\text{OH})_8$, $\text{ScTi}_{15}\text{C}_8\text{O}_{12}(\text{OH})_4$ and $\text{ScTi}_{15}\text{C}_8\text{O}_4(\text{OH})_{12}$, respectively. For Sc

substitution in $2 \times 2 \times 1$ - $\text{Ti}_2\text{CO}_x\text{F}_y$ systems, the magnetic moments of $\text{ScTi}_{15}\text{C}_8\text{O}_8\text{F}_8$, $\text{ScTi}_{15}\text{C}_8\text{O}_{12}\text{F}_4$ and $\text{ScTi}_{15}\text{C}_8\text{O}_4\text{F}_{12}$ are 7.00, 3.00 and 11.00 μ_B/cell , respectively. On the other hand, the introduction of Sc atom in the cell introduce a charge/spin redistribution keeping the magnetic moment in the same order as the structures without Ti substitution by Sc. The absolute value of magnetic moments of the carbon atoms slightly increased in all structures by the substitution (Please see Table S2 and Table S3 in the ESI). Remarkably, the introduction of one Sc in $\text{Ti}_2\text{CF}_{1.0}(\text{OH})_{1.0}$ (i.e., $\text{ScTi}_{15}\text{C}_8\text{F}_8(\text{OH})_8$) and $\text{Ti}_2\text{CF}_{1.5}(\text{OH})_{0.5}$ (i.e., $\text{ScTi}_{15}\text{C}_8\text{F}_4(\text{OH})_4$) makes a magnetic transition from AFM alignment to ferrimagnetic (FiM) ordering and the local magnetic moment were induced in the C atoms in the order of 0.6 to 0.75 μ_B . Moreover, the value of the local magnetic moments on Sc atoms is slightly low (in the order of 0.14 and 0.18 μ_B).

Table 2 Calculated total magnetic moments of $2 \times 2 \times 1$ - $\text{Ti}_2\text{CA}_x\text{B}_y$ (A, B = O, F, OH) with one Ti substituted by Sc.

Structure	Magnetic moment (μ_B/cell)
$\text{ScTi}_{15}\text{C}_8\text{O}_8(\text{OH})_8$	7.04
$\text{ScTi}_{15}\text{C}_8\text{O}_{12}(\text{OH})_4$	3.21
$\text{ScTi}_{15}\text{C}_8\text{O}_4(\text{OH})_{12}$	11.23
$\text{ScTi}_{15}\text{C}_8\text{O}_8\text{F}_8$	7.00
$\text{ScTi}_{15}\text{C}_8\text{O}_{12}\text{F}_4$	3.00
$\text{ScTi}_{15}\text{C}_8\text{O}_4\text{F}_{12}$	11.00
$\text{ScTi}_{15}\text{C}_8\text{F}_8(\text{OH})_8$	14.97
$\text{ScTi}_{15}\text{C}_8\text{F}_{12}(\text{OH})_4$	5.00
$\text{ScTi}_{15}\text{C}_8\text{F}_4(\text{OH})_{12}$	15.06

3.3 Substitution of Ti by Sc in Ti_2CO_2

In our previous study¹⁴, we show that the presence of C-vacancy in Ti_2CO_2 induces magnetism in the system. Moreover, as we noticed above, there is some effect of Sc atom in Ti_2C -based MXene structures (cf. Section 3.1 and 3.2). We therefore decided to investigate also the effect of Sc substitution in a bare Ti_2CO_2 MXene. Here, we investigate the effect of the substitution of the transition metal (Ti) by Sc in $5 \times 5 \times 1$ - Ti_2CO_2 ; i.e., $\text{Sc}_n\text{Ti}_{50-n}\text{C}_{25}\text{O}_{50}$ structure, where $n = 1, 2, 3, 4, 5, 6$, and 7.

Table 3 Calculated magnetic moments (in μ_B/cell) of Ti substituted by Sc in $5 \times 5 \times 1$ - Ti_2CO_2 on different directions (Zigzag, Armchair and Cluster). NM refers to nonmagnetic.

	Zigzag	Armchair	Cluster
1Sc	0.00 (NM)	0.00 (NM)	0.00 (NM)
2Sc	0.16	0.16	0.16
3Sc	0.18	0.18	0.18
4Sc	0.00 (NM)	0.00 (NM)	0.00 (NM)
5Sc	1.05	0.00 (NM)	0.96
6Sc	2.08	0.00 (NM)	1.98
7Sc	3.07	1.78	-

In the Table 3, we show the calculated magnetic moments in Ti_2CO_2 supercell after the substitution of n Ti atom by n Sc atoms. In our study, we have found that by substituting only one Ti by Sc, the structure remain nonmagnetic (NM). By increasing the

number of Sc atoms in the supercell, the magnetism is turned on, but some structures keep a nonmagnetic (NM) behavior, more precisely, when substituting 4 Ti atoms with Sc, and also when substituting 5 and 6 Ti atoms with Sc along the armchair direction. Substitution induces local magnetic moments from $0.16\mu_B$ to about $3\mu_B$ in the supercell depending on the position and the number of Sc in the system.

We note that for the magnetic structure, 5 and 6 Sc in $5\times 5\times 1$ - Ti_2CO_2 in the zigzag direction are more preferred over the cluster form by an energy difference of 0.08 eV and 0.24 eV, respectively. While 7Sc in armchair are more stable compared to the zigzag direction, the energy difference is 0.32 eV. The total energies of n Ti atoms substituted by n Sc atoms in $5\times 5\times 1$ - Ti_2CO_2 following the Zigzag, Armchair, and Cluster directions are listed in Table S2.

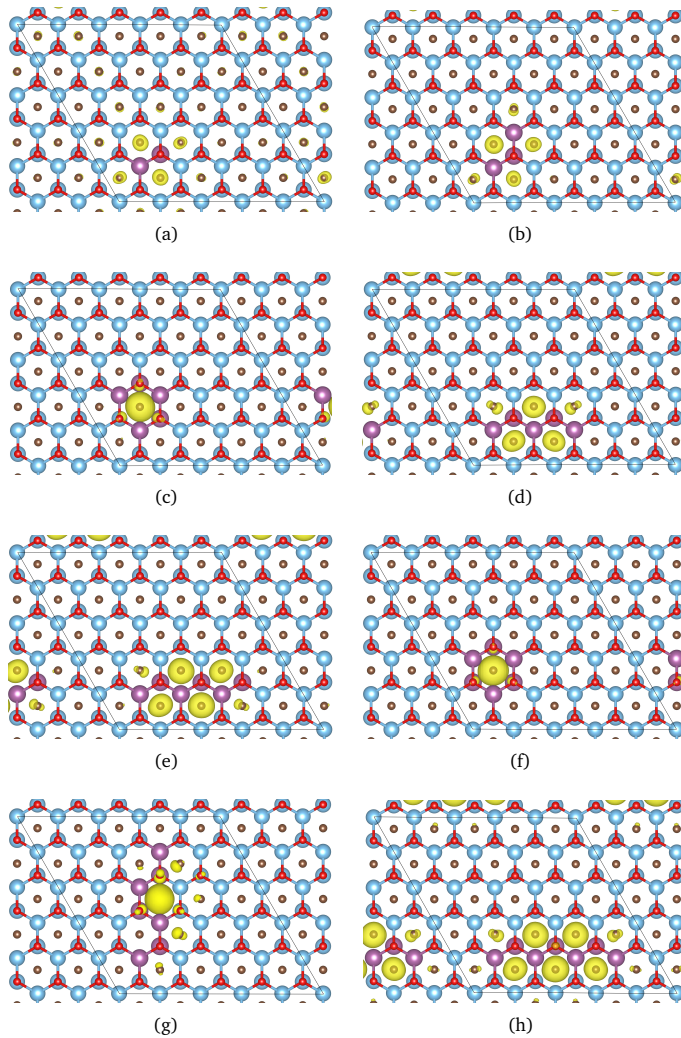


Fig. 5 Spin density distribution of n Ti atoms substituted by n Sc atoms in $5\times 5\times 1$ - Ti_2CO_2 , $n=2, 3, 5, 6$, and 7 . (a) 2 Sc atoms and (b) 3 Sc atoms using isosurface $=10^{-3}$ au and (c) 5 Sc atoms (cluster) (d) 5 Sc atoms (zigzag direction) (e) 6 Sc atoms (zigzag direction) (f) 6 Sc atoms (cluster) (g) 7 Sc atoms (armchair direction), and (h) 7 Sc atoms (zigzag direction) with isosurface $=5\times 10^{-3}$ au. Yellow color represents the spin density. Blue, red, chocolate and violet balls refer to Ti, O, C and Sc atoms, respectively. The plots were produced by using VESTA software⁶².

To pick up more knowledge into the magnetic properties, the spin electron density distributions of n Sc atoms in $\text{Ti}_{50}\text{C}_{25}\text{O}_{50}$ are computed and compared in Fig. 5. The results indicate that the spin density is almost entirely localized around C atoms that are close to the Sc atoms. There is no spin density in the rest of the supercell, which confirm that the incorporation of the Sc atom make a charge rearrangement around the surrounding atoms and therefore, magnetism is induced. It is shown that the induced magnetism is mainly attributed the Sc since the spin electrons are mostly concentrated on the surrounding of Sc atoms. Moreover, some fraction of spin density are located at C atoms.

4 Conclusion

The electronic structure and magnetic properties of mixed termination in Ti_2C MXenes have been studied by DFTB method using the recently developed xTB Hamiltonian. $\text{Ti}_2\text{CA}_x\text{B}_y$ ($A, B = \text{O, F, OH}$) monolayers show spin polarization and the magnetic alignment depends on the mixed termination. Ferromagnetic (FM) ordering appears in most of compositions except $\text{Ti}_2\text{CF}_1(\text{OH})_1$ and $\text{Ti}_2\text{CF}_{1.5}(\text{OH})_{0.5}$, which are antiferromagnetic (spin orientations of metal atoms on one side are opposite to those on the other side; AFM2 arrangement). The effect of the transition metal atom (Ti) substituted by the another one (Sc atom) on the electronic and magnetic properties were modeled by $2\times 2\times 1$ - $\text{Ti}_2\text{CA}_x\text{B}_y$ supercell. A ferrimagnetic (FiM) alignment was found and a charge/spin redistribution was introduced which explain the slight change of the total magnetic moments compared to the structures without Sc atoms. Interestingly, a magnetic transition from AFM to FiM was found for $\text{ScTi}_{15}\text{C}_8\text{F}_8(\text{OH})_8$ and $\text{ScTi}_{15}\text{C}_8\text{F}_{12}(\text{OH})_4$. We also investigated the effect of substitution of n Ti atoms by n Sc atoms in the fully O-terminated Ti_2CO_2 MXene following different configuration, including cluster, armchair, and zigzag direction. We found that magnetism is tuned by the Sc substitution in $\text{Ti}_{50}\text{C}_{25}\text{O}_{50}$ and it is sensitive to the number of Sc atoms in the cell and to the direction of the substituent. In the magnetic structures, the total magnetic moment is higher for higher number of Sc in the cell. Moreover, the shown half-metallicity ferromagnetism and metallicity antiferromagnetism in $\text{Ti}_2\text{CA}_x\text{B}_y$ and Ti_2CO_2 may provide more potential applications in spintronic devices.

Finally, we conclude that the recent GFN1-xTB Hamiltonian is useful for the investigation of the electronic and magnetic properties of MXenes. However, further targeted studies are required to conclude about it's utilization for the modeling of the 2D materials and periodic systems of big sizes.

Conflicts of interest

There is no conflict to declare.

Acknowledgements

This article has been produced with the financial support of the Czech Science Foundation (21-28709S) and the European Union under the LERCO project (number CZ.10.03.01/00/22_003/0000003) via the Operational Programme Just Transition. The computations were performed at IT4Innovations National Supercomputing Center through the e-

References

- 1 B. Anasori and Y. Gogotsi, Graphene and 2D Materials, 2022, 75 – 79.
- 2 B. Anasori, M. R. Lukatskaya and Y. Gogotsi, Nat. Rev. Mater., 2017, **2**, 16098.
- 3 Y. Zhang, X.-H. Zha, K. Luo, N. Qiu, Y. Zhou, J. He, Z. Chai, Z. Huang, Q. Huang, Y. Liang and S. Du, J. Phys. Chem. C, 2019, **123**, 6802 – 6811.
- 4 M. A. Hope, A. C. Forse, K. J. Griffith, M. R. Lukatskaya, M. Ghidui, Y. Gogotsi and C. P. Grey, Phys. Chem. Chem. Phys., 2016, **18**, 5099–5102.
- 5 Y. Zhang, W. Xia, Y. Wu and P. Zhang, Nanoscale, 2019, **11**, 3993–4000.
- 6 M. Naguib, M. Kurtoglu, V. Presser, J. Lu, J. Niu, M. Heon, L. Hultman, Y. Gogotsi and M. W. Barsoum, Adv. Mater., 2011, **23**, 4248–4253.
- 7 P. Johari and V. B. Shenoy, ACS Nano, 2011, **5**, 7640–7647.
- 8 K. J. Harris, M. Bugnet, M. Naguib, M. W. Barsoum and G. R. Goward, J. Phys. Chem. C, 2015, **119**, 13713 – 13720.
- 9 H.-H. Wang, Y.-L. Cui, N. G. Zaorsky, J. Lan, L. Deng, X.-L. Zeng, Z.-Q. Wu, Z. Tao, W.-H. Guo, Q.-X. Wang and *et al.*, Cancer Lett., 2016, **375**, 349–359.
- 10 L. H. Karlsson, J. Birch, J. Halim, M. W. Barsoum and P. O. A. Persson, Nano Lett., 2015, **15**, 4955 – 4960.
- 11 M. Khazaei, M. Arai, T. Sasaki, C.-Y. Chung, N. S. Venkataramanan, M. Estili, Y. Sakka and Y. Kawazoe, Adv. Funct. Mater., 2013, **23**, 2185–2192.
- 12 C. Wang, H. Han and Y. Guo, Comput. Mater. Sci., 2019, **159**, 127–135.
- 13 T. Ketolainen and F. Karlický, J. Mater. Chem. C, 2022, **10**, 3919–3928.
- 14 T. Sakhraoui and F. Karlický, ACS Omega, 2022, **7**, 42221.
- 15 M. Dubecký, S. Minárik and F. Karlický, J. Chem. Phys., 2023, **158**, 054703.
- 16 N. Kumar and F. Karlický, Appl. Phys. Lett., 2023, **122**, 183102.
- 17 S. Sarikurt, D. Çakır, M. Keçeli and C. Sevik, Nanoscale, 2018, **10**, 8859–8868.
- 18 T. Hu, J. Yang and X. Wang, Phys. Chem. Chem. Phys., 2017, **19**, 31773–31780.
- 19 X. Guo, P. Zhang and J. Xue, J. Phys. Chem. Lett., 2016, **7**, 5280–5284.
- 20 Q. Hu, D. Sun, Q. Wu, H. Wang, L. Wang, B. Liu, A. Zhou and J. He, J. Phys. Chem. A, 2013, **117**, 14253–14260.
- 21 G. Gao, G. Ding, J. Li, K. Yao, M. Wu and M. Qian, Nanoscale, 2016, **8**, 8986–8994.
- 22 S. A. Khan, B. Amin, L.-Y. Gan and I. Ahmad, Phys. Chem. Chem. Phys., 2017, **19**, 14738–14744.
- 23 Y. Zhang, X.-H. Zha, K. Luo, N. Qiu, Y. Zhou, J. He, Z. Chai, Z. Huang, Q. Huang, Y. Liang and S. Du, J. Phys. Chem. C, 2019, **123**, 6802–6811.
- 24 H. Ahmad, M. J. Mohd Makhfuz, N. Yusoff, A. D. Azam and M. Z. Samion, Optical Materials, 2023, **135**, 113340.
- 25 X.-H. Zha, K. Luo, Q. Li, Q. Huang, J. He, X. Wen and S. Du, Europhysics Letters, 2015, **111**, 26007.
- 26 R. Ibragimova, M. J. Puska and H.-P. Komsa, ACS Nano, 2019, **13**, 9171 – 9181.
- 27 M. Li, X. Li, G. Qin, K. Luo, J. Lu, Y. Li, G. Liang, Z. Huang, J. Zhou, L. Hultman, P. Eklund, P. O. A. Persson, S. Du, Z. Chai, C. Zhi and Q. Huang, ACS Nano, 2021, **15**, 1077 – 1085.
- 28 K. Kawai, M. Fujita, R. Iizuka, A. Yamada and M. Okubo, 2D Materials, 2022, **10**, 014012.
- 29 S.-Y. Pang, Y.-T. Wong, S. Yuan, Y. Liu, M.-K. Tsang, Z. Yang, H. Huang, W.-T. Wong and J. Hao, Journal of the American Chemical Society, 2019, **141**, 9610–9616.
- 30 M. Li, J. Lu, K. Luo, Y. Li, K. Chang, K. Chen, J. Zhou, J. Rosen, L. Hultman, P. Eklund, P. O. A. Persson, S. Du, Z. Chai, Z. Huang and Q. Huang, Journal of the American Chemical Society, 2019, **141**, 4730–4737.
- 31 V. Kamysbayev, A. S. Filatov, H. Hu, X. Rui, F. Lagunas, D. Wang, R. F. Klie and D. V. Talapin, Science, 2020, **369**, 979–983.
- 32 N. Garcia-Romeral, A. Morales-Garcia, F. Vines, I. d. P. R. Moreira and F. Illas, The Journal of Physical Chemistry C, 2023, **127**, 3706 – 3714.
- 33 S. Bae, Y.-G. Kang, M. Khazaei, K. Ohno, Y.-H. Kim, M. Han, K. Chang and H. Raebiger, Materials Today Advances, 2021, **9**, 100118.
- 34 C. Jin, J. Shang, X. Tang, X. Tan, S. C. Smith, C. Niu, Y. Dai and L. Kou, J. Mater. Chem. C, 2019, **7**, 15308–15314.
- 35 A. N. Enyashin and A. L. Ivanovskii, The Journal of Physical Chemistry C, 2013, **117**, 13637 – 13643.
- 36 X. Sang, Y. Xie, M.-W. Lin, M. Alhabeab, K. L. Van Aken, Y. Gogotsi, P. R. C. Kent, K. Xiao and R. R. Unocic, ACS Nano, 2016, **10**, 9193 – 9200.
- 37 M. Bagheri, R. Ibragimova and H.-P. Komsa, Phys. Rev. B, 2021, **104**, 035408.
- 38 T. Hu, M. Hu, B. Gao, W. Li and X. Wang, J. Phys. Chem. C, 2018, **122**, 18501 – 18509.
- 39 T. Schultz, N. C. Frey, K. Hantanasirisakul, S. Park, S. J. May, V. B. Shenoy, Y. Gogotsi and N. Koch, Chem. Mater., 2019, **31**, 6590 – 6597.
- 40 A. S. Christensen, T. Kubař, Q. Cui and M. Elstner, Chem. Rev., 2016, **116**, 5301 – 5337.
- 41 M. Haugk, J. Elsner, T. Frauenheim, T. Staab, C. Latham, R. Jones, H. Leipner, T. Heine, G. Seifert and M. Sternberg, physica status solidi (b), 2000, **217**, 473–511.
- 42 M. Elstner, T. Frauenheim, E. Kaxiras, G. Seifert and S. Suhai, physica status solidi (b), 2000, **217**, 357–376.
- 43 Y. A. Çetin, B. Martorell, F. Serratos, N. Aguilera-Porta and M. Calatayud, J. Phys.: Condens. Matter, 2022, **34**, 314004.
- 44 T. Sakhraoui and F. Karlický, Phys. Chem. Chem. Phys., 2022, **24**, 3312–3321.
- 45 H. Manzano, A. N. Enyashin, J. S. Dolado, A. Ayuela, J. Frenzel and G. Seifert, Advanced Materials, 2012, **24**, 3239–3245.
- 46 Y. Nishimura and H. Nakai, Journal of Computational

- Chemistry, 2019, **40**, 1538–1549.
- 47 A. S. Hutama, L. A. Marlina, C.-P. Chou, S. Irle and T. S. Hofer, ACS Omega, 2021, **6**, 20530 – 20548.
- 48 G. Budiutama, R. Li, S. Manzhos and M. Ihara, Journal of Chemical Theory and Computation, 2023, **19**, 5189 – 5198.
- 49 A. N. Kocharian, G. W. Fernando, K. Palandage and J. W. Davenport, Phys. Rev. B, 2006, **74**, 024511.
- 50 O. M. Auslaender, A. Yacoby, R. de Picciotto, K. W. Baldwin, L. N. Pfeiffer and K. W. West, Phys. Rev. Lett., 2000, **84**, 1764–1767.
- 51 M. Sassetti and B. Kramer, Phys. Rev. Lett., 1998, **80**, 1485–1488.
- 52 F. Lopez-Urias, E. Cruz-Silva, E. Munoz-Sandoval, M. Terrones and H. Terrones, J. Mater. Chem., 2008, **18**, 1535–1541.
- 53 S. Grimme, C. Bannwarth and P. Shushkov, J. Chem. Theory Comput., 2017, **13**, 1989 – 2009.
- 54 B. Hourahine, B. Aradi, V. Blum, F. Bonafé, A. Buccheri, C. Camacho, C. Cevallos, M. Y. Deshayé, T. Dumitrică, A. Dominguez, S. Ehlert, M. Elstner, T. van der Heide, J. Hermann, S. Irle, J. J. Kranz, C. Köhler, T. Kowalczyk, T. Kubař, I. S. Lee, V. Lutsker, R. J. Maurer, S. K. Min, I. Mitchell, C. Negre, T. A. Niehaus, A. M. N. Niklasson, A. J. Page, A. Pecchia, G. Penazzi, M. P. Persson, J. Řezáč, C. G. Sánchez, M. Sternberg, M. Stöhr, F. Stuckenberg, A. Tkatchenko, V. W.-z. Yu and T. Frauenheim, J. Chem. Phys., 2020, **152**, 124101.
- 55 M. Nurhuda, C. C. Perry and M. A. Addicoat, Phys. Chem. Chem. Phys., 2022, **24**, 10906–10914.
- 56 J. P. Menzel, M. Kloppenburg, J. Belić, H. J. M. de Groot, L. Visscher and F. Buda, Journal of Computational Chemistry, 2021, **42**, 1885–1894.
- 57 C. Bannwarth, E. Caldeweyher, S. Ehlert, A. Hansen, P. Pracht, J. Seibert, S. Spicher and S. Grimme, WIREs Computational Molecular Science, 2021, **11**, e1493.
- 58 C. Bannwarth, S. Ehlert and S. Grimme, J. Chem. Theory Comput., 2019, **15**, 11652 – 1671.
- 59 B. Aradi, B. Hourahine and T. Frauenheim, J. Phys. Chem. A, 2007, **111**, 5678–5684.
- 60 J. M. Vicent-Luna, S. Apergi and S. Tao, J. Chem. Inf. Model., 2021, **61**, 4415 – 4424.
- 61 H. J. Monkhorst and J. D. Pack, Phys. Rev. B, 1976, **13**, 5188–5192.
- 62 K. Momma and F. Izumi, Journal of Applied Crystallography, 2011, **44**, 1272–1276.